Using machine learning to parameterize moist convection: potential for modeling of climate, climate change and extreme events

Paul A. O'Gorman[1], John G. Dwyer[1]*

[1]Department of Earth, Atmospheric and Planetary Sciences, Massachusetts Institute of Technology, Cambridge, Massachusetts 02139, USA.

Key Points:

- Random-forest parameterization of convection gives accurate GCM simulations of climate and precipitation extremes in idealized tests
- Climate change captured when trained on control and warm climate, or only on warm climate, but not when trained only on control climate
- Machine-learning parameterizations can also be interrogated to generate diagnostics of interaction of convection with the environment

---

*Current address: Dia&Co, New York

Corresponding author: Paul A. O'Gorman, `pog@mit.edu`

Abstract

The parameterization of moist convection contributes to uncertainty in climate modeling and numerical weather prediction. Machine learning (ML) can be used to learn new parameterizations directly from high-resolution model output, but it remains poorly understood how such parameterizations behave when fully coupled in a general circulation model (GCM) and whether they are useful for simulations of climate change or extreme events. Here, we focus on these issues using idealized tests in which an ML-based parameterization is trained on output from a conventional parameterization and its performance is assessed in simulations with a GCM. We use an ensemble of decision trees (random forest) as the ML algorithm, and this has the advantage that it automatically ensures conservation of energy and non-negativity of surface precipitation. The GCM with the ML convective parameterization runs stably and accurately captures important climate statistics including precipitation extremes without the need for special training on extremes. Climate change between a control climate and a warm climate is not captured if the ML parameterization is only trained on the control climate, but it is captured if the training includes samples from both climates. Remarkably, climate change is also captured when training only on the warm climate, and this is because the extratropics of the warm climate provides training samples for the tropics of the control climate. In addition to being potentially useful for the simulation of climate, we show that ML parameterizations can be interrogated to provide diagnostics of the interaction between convection and the large-scale environment.

1 Introduction

General circulation models (GCMs) of the atmosphere and ocean are important tools for climate simulation and numerical weather prediction. GCMs are based on equations describing resolved dynamics (using the laws of conservation of energy, momentum and mass) and parameterization schemes that represent subgrid processes. Parameterization schemes are necessary because there are insufficient computational resources to resolve all relevant length and time scales, but they are also the source of considerable uncertainties and biases [e.g., *Wilcox and Donner*, 2007; *Bechtold et al.*, 2008; *Farneti and Gent*, 2011; *Stevens and Bony*, 2013].

One potential way forward is to use machine learning (ML) to create new parameterization schemes by fitting a statistical model to the output of relatively expensive physical models that more faithfully represent the subgrid dynamics. By minimizing the error between an ML model's predictions and the known output over many training examples, ML models can learn complex mappings without being explicitly programmed. ML-based parameterizations have been developed for radiative transfer [e.g., *Chevallier et al.*, 1998; *Belochitski et al.*, 2011] and for convective and boundary-layer processes [*Krasnopolsky et al.*, 2010, 2013; *Brenowitz and Bretherton*, 2018; *Gentine et al.*, 2018; *Rasp et al.*, 2018]. The use of ML is also currently being explored for subgrid turbulence modeling for engineering applications [e.g., *Ling et al.*, 2016; *Wang et al.*, 2017].

In contrast to conventional parameterizations, an ML-based parameterization takes a statistical approach and need not assume a simplified physical model such as the entraining plume that is often used in convective parameterizations. The resulting GCM is then a hybrid model consisting of a physically-based component and one or more ML-based components [*Krasnopolsky*, 2013]. Such a hybrid approach is particularly attractive if the most uncertain parameterizations in GCMs (which often include many tunable parameters) can be replaced with ML-based parameterizations that are training systematically. An alternative approach to leveraging high-resolution modeling or observations would be to use them to optimize parameters while still retaining a physically-based subgrid model [cf. *Emanuel and Živković-Rothman*, 1999; *Schneider et al.*, 2017].

Subgrid moist convection is a good candidate for ML parameterization because cloud-system resolving model (CRM) simulations are available to generate training data, and be-

cause conventional parameterizations for moist convection are responsible for considerable uncertainty in global modeling of the atmosphere. Ideally a convective parameterization will accurately represent the subgrid fluxes of moisture, temperature and momentum associated with convective instability, and account for both updrafts and downdrafts, mixing with the environment, and cloud microphysical processes. Historically a wide range of approaches have been used to parameterize moist convection [e.g., *Arakawa*, 2004]. Recent developments include efforts to include the effects of the spatial organization of convection [*Mapes and Neale*, 2011] and use of super-parameterization in which CRMs are embedded in GCM grid boxes [*Khairoutdinov and Randall*, 2001; *Randall et al.*, 2003]. Convective parameterizations affect the vertical structure of temperature and humidity in the tropics [*Held et al.*, 2007; *Benedict et al.*, 2013] and the ability of GCMs to simulate the Madden Julian Oscillation and other tropical disturbances [*Kim et al.*, 2012; *Benedict et al.*, 2013]. Convective parameterizations also strongly affect how precipitation extremes are simulated [*Wilcox and Donner*, 2007] and this helps to explain the large spread in projected changes in precipitation extremes in the tropics [*O'Gorman*, 2012].

CRM simulations differ from convective parameterizations in their predictions for the response of convective tendencies to perturbations in temperature and moisture, both in terms of magnitude and vertical structure [*Herman and Kuang*, 2013]. Furthermore, super-parameterization using embedded CRMs can reduce biases in GCM simulations [e.g., *Kooperman et al.*, 2016]. Thus, it is plausible that ML parameterizations learned from CRM simulations could outperform conventional parameterizations, and a GCM with an ML parameterization would be much faster than a global CRM.

In a pioneering study, *Krasnopolsky et al.* [2013] used an ensemble of shallow artificial neural networks (ANNs) to learn temperature and moisture tendencies from CRM simulations forced by observations from a region of the equatorial Pacific. Tendencies from the resulting convective parameterization were compared to tendencies from a conventional parameterization over the tropical Pacific in a diagnostic test, but the key issue of fully coupling the ML-based convection parameterization to the GCM was not addressed. Two recent studies, published while this paper was in review, have found that a parameterization of subgrid processes based on a shallow ANN ran stably in prognostic single-column integrations when the loss function included many time steps [*Brenowitz and Bretherton*, 2018], and that a deep ANN trained on tendencies from a superparameterized GCM lead to stable and accurate integrations in the same GCM [*Rasp et al.*, 2018].

Here, we use idealized tests to explore the potential of ML-based parameterization for simulations of climate and climate change, and we demonstrate ways in which the ML-based parameterization can be used to gain physical insight into the interaction of convection with its environment. We train an ML-based parameterization on the output of a conventional moist-convective parameterization, the relaxed Arakawa-Schubert (RAS) scheme [*Moorthi and Suarez*, 1992]. We then implement the ML-based parameterization in simulations with an idealized GCM and compare the results to simulations with RAS. This "perfect-parameterization" approach provides us with a simple testbed in which we can cleanly investigate a number of important questions concerning how an ML-based parameterization behaves when implemented in a GCM. As described in detail in *Moorthi and Suarez* [1992], RAS is based on a spectrum of entraining plumes and shares many features with real convection such as sensitivity to humidity and temperature and nonlinear behavior such as only being active under certain conditions. Since RAS is not stochastic and is local in time and space, the idealized tests considered here may be viewed as a best-case deterministic scenario for column-based machine learning that does not include the effect of neighboring grid cells or past conditions.

We use a random forest (RF) [*Breiman*, 2001; *Hastie et al.*, 2001] to learn the outputs of the RAS convection scheme which are the convective tendencies of temperature and specific humidity. Because we train on the output of RAS, the surface precipitation rate is implied by the mass-weighted vertical integral of the specific humidity tendency and does not

have to be predicted separately. The RF consists of an ensemble of decision trees, and each tree makes predictions that are means over subsets of the training data. The final prediction from the RF is the average over all trees. As described in the next section, the RF has attractive properties for the parameterization problem in terms of preserving physical constraints such as energy conservation, and we will show that it leads to accurate and stable simulations of climate in the GCM. Running in a GCM is a non-trivial test of an ML parameterization because errors in the parameterization could push the temperature and humidity outside the domain of the training data as the GCM is integrated forward in time leading to large extrapolation errors [cf. *Krasnopolsky et al.*, 2008; *Brenowitz and Bretherton*, 2018]. We also initially experimented with using shallow ANNs (e.g., a single hidden layer with 60 neurons), but we found that the resulting parameterization was less robust than the RF and did not conserve energy without a post-prediction correction. We do not discuss these ANN results further given recent advances using different ANN training approaches and architectures [*Brenowitz and Bretherton*, 2018; *Rasp et al.*, 2018], and we instead focus on our promising results for the RF parameterization.

In addition to investigating the ability of the GCM with the RF parameterization to accurately simulate basic statistics of a control climate, we also investigate whether it accurately simulates extreme precipitation events and climate change. For extreme events, we show that special training is not needed to correctly capture the statistics of these events. For climate change, we expect that an ML parameterization trained on a control climate would not be able to generalize to a different climate to the extent that this requires extrapolation beyond the training data. Thus, the extent to which generalization is successful can depend on both the magnitude of the climate change and the range of unforced variability in the control climate. Interestingly, we also show that whether the climate is warming or cooling is important, and that generalization across climates is related to generalization across latitudes. It is also important to know whether training one parameterization on a combination of different climate states will work well since this would be necessary for transient climate-change simulations. Note that training on different climates is possible when training is based on model output (e.g., from a global CRM) as long as these simulations can be run for a sufficiently long period in a different climate.

Another promising aspect of ML is that it can be used to gain insight from large datasets into underlying physical processes [e.g., *Monteleoni et al.*, 2013]. Here, we explore whether the RF parameterization can be analyzed to provide insights into the interaction of convection with the environment. We consider both the linear sensitivity as has been previously discussed for moist convection [*Kuang*, 2010; *Herman and Kuang*, 2013; *Mapes et al.*, 2017], and feature importance which is a common concept in ML [*Hastie et al.*, 2001] that does not require an assumption of small perturbations.

We begin by describing the RF algorithm (section 2), the RAS convection scheme and idealized GCM simulations used to generate training datasets (section 3), and the training and validation of the RF convection scheme (section 4). We discuss the ability of the idealized GCM with the RF scheme to reproduce the control climate including the mean state and extremes (section 5), and its ability to capture climate change given different approaches to training (section 6). We also show how the RF scheme can be used to provide insight into the importance of the environmental temperature and humidity at different vertical levels for convection (section 7). Lastly, we briefly discuss the ability of the RF scheme to represent the combination of the convection and large-scale condensation schemes (section 8) before giving our conclusions (section 9).

2 Machine learning algorithm: random forest

A random forest (RF) is a machine-learning estimator that consists of an ensemble of decision trees [*Breiman*, 2001; *Hastie et al.*, 2001]. RFs are widely used because they do not require much preprocessing and they generally perform well over a wide range of hy-

perparameters. The inputs to the RF are referred to as features, and each decision tree is a recursive binary partition of the feature space. Each leaf of the tree contains a prediction for the output variables that for continuous output variables is taken to be the mean over the output from the training samples in that leaf. Predictions of an RF are the mean of the predictions across all the trees, and the purpose of having multiple trees is to reduce the variance of the prediction since individual decision trees are prone to overfitting. The different trees are created by bootstrapping of the training data and by only considering a randomly chosen subset of one third of the features at each split when constructing the trees. The alternative approach of considering all of the features at each split, referred to as bagging, gives similar test scores for the problem investigated here.

Training of the RF is an example of supervised learning in which an ML algorithm and a training dataset are used to learn a mapping between features and outputs [e.g., *Hastie et al.*, 2001]. The aim of the training is to minimize the mean squared error between the known and predicted outputs, and the resulting model is referred to as a regression model because it predicts continuous variables. Details of the features used and training of the RF are given in section 4.

One major advantage of using an RF is that predictions are means over subsets of the training data, and this leads to exact conservation of energy and non-negativity of surface precipitation by the RF parameterization. Non-negativity of surface precipitation follows immediately since the training samples all have non-negative precipitation, and the mean of a set of non-negative numbers is a non-negative number. To conserve energy in a hydrostatic GCM, a convective parameterization that neglects convective momentum transports should conserve column-integrated moist enthalpy, and this is the case for RAS. Moist enthalpy is a linear function of temperature and specific humidity in our GCM, and thus the predicted tendency by the RF of the vertically-integrated moist enthalpy will be zero, ensuring energy conservation. One disadvantage of the RF is that considerable memory must be available when running the GCM in order to store the tree structures and predicted values.

The property that the RF predictions are averages over subsets of the training data may also improve the robustness and stability of the RF when implemented in the GCM. In particular, the predicted convective tendencies cannot differ greatly from those in the training data, even if the RF is applied to input temperature and humidity profiles that require extrapolation outside of the training data (as can occur when an ML parameterization is implemented in a GCM).

3 Convection scheme and idealized GCM simulations

Our approach is to use a relatively complex convection scheme, typical of those used in current climate models, and implement it in an idealized GCM configuration to simplify the analysis of climate and climate change. The idealized GCM allows us to investigate the interaction between resolved dynamics and convection, but it does not include important complicating factors such as the diurnal cycle over land and cloud-radiation interactions.

For the convection scheme, we use the version of RAS that was implemented in the GFDL AM2 model [*Anderson et al.*, 2004]. This scheme is an efficient variant of the Arakawa-Schubert scheme [*Arakawa and Schubert*, 1974] in which the cloud ensemble is relaxed towards quasi-equilibrium. The basis of the scheme is an ensemble of entraining plumes that represent both shallow and deep convection. As discussed in *Held et al.* [2007], the AM2 version of the scheme includes an entrainment limiter that is only active for deep convection. The inputs to RAS are the vertical profiles of temperature and specific humidity as a function of pressure, and the outputs are the tendencies of temperature and specific humidity. We do not consider convective momentum tendencies.

The idealized GCM is an atmospheric model based on a version of the GFDL spectral dynamical core coupled to a shallow thermodynamic mixed-layer ocean of depth 0.5m.

There is no land or ice, and no seasonal or diurnal cycles. The GCM is similar to that of *Frierson et al.* [2006] with the details as in *O'Gorman and Schneider* [2008] except that here we use the RAS convection scheme and we allow evaporation of falling condensate in the large-scale condensation scheme. The top-of-atmosphere insolation is imposed as a perpetual equinox distribution. Longwave radiation is represented by a two-stream gray scheme with prescribed optical thickness as a function of latitude and pressure, and there are no water-vapor or cloud radiative feedbacks. The spectral resolution is T42, there are 30 vertical sigma levels, and the time step is 10 minutes. The RAS scheme is responsible for most of the mean precipitation in the tropics, with the large-scale condensation scheme contributing to a greater extent at middle and high latitudes. This idealized GCM configuration (but with a simpler convection scheme) has previously been found to be useful for investigations of moist atmospheric dynamics and the response of precipitation to climate change [e.g., *O'Gorman and Schneider*, 2009; *O'Gorman*, 2011; *Dwyer and O'Gorman*, 2017].

The simulations with the RAS convection scheme are spun up over 700 days from an isothermal rest state to reach statistical equilibrium. The simulations are then run for a subsequent 3300 days, and this period is used to build training datasets for ML as described in the next section. Simulations with the RF-based convection scheme are spun up over 700 days from the statistical equilibrium state of the corresponding RAS simulation and then run for a subsequent 900 days. Simulations without any convection scheme are also used for comparison purposes, and these are spun up over 700 days from an isothermal rest state. All figures that present climate statistics are based on 900 days at statistical equilibrium. The lower boundary condition and the top-of-atmosphere insolation are zonally and hemispherically symmetric, and thus differences between the hemispheres in figures are indicative of sampling errors, except for the climate-change results in which the fields have been symmetrized between the hemispheres to reduce noise.

We consider two climates: a control climate with a global-mean surface air temperature of 288K (similar to the reference climate in *O'Gorman and Schneider* [2008]), and a warm climate with a global-mean surface air temperature of 295K that is obtained by increasing the longwave optical thickness by a factor of 1.4 to mimic a large increase in greenhouse-gas concentrations.

4 Training and validation of the random forest

4.1 Features and outputs

The features are the inputs to the RF, and they are chosen here to be the vertical profiles of temperature and specific humidity (discretized at the vertical σ levels) and the surface pressure. Given that σ is pressure normalized by surface pressure, these features are equivalent to the inputs to RAS which are the vertical profiles of temperature and specific humidity as a function of pressure. Tests in which surface pressure is not included as a feature in the RF gave similar performance (note that the idealized GCM does not include topography). We do not include surface fluxes as features since these are not an input to the RAS convection scheme.

The outputs are the vertical profiles of the convective tendencies of temperature and specific humidity. Cumulus momentum transports and interactions of convection with radiation are not predicted since these are not included in the idealized GCM. The choice of output scaling for temperature versus humidity tendencies affects how the RF fits the training data. We chose to multiply the temperature tendencies by the specific heat capacity of air at constant pressure (c_p), and the specific humidity tendencies by the latent heat of condensation (L) to give the same units for both tendencies. The quality of the fit is similar if each output is instead standardized by removing the mean and rescaling to unit variance. The training aims to minimize the mean squared error summed over all the scaled outputs.
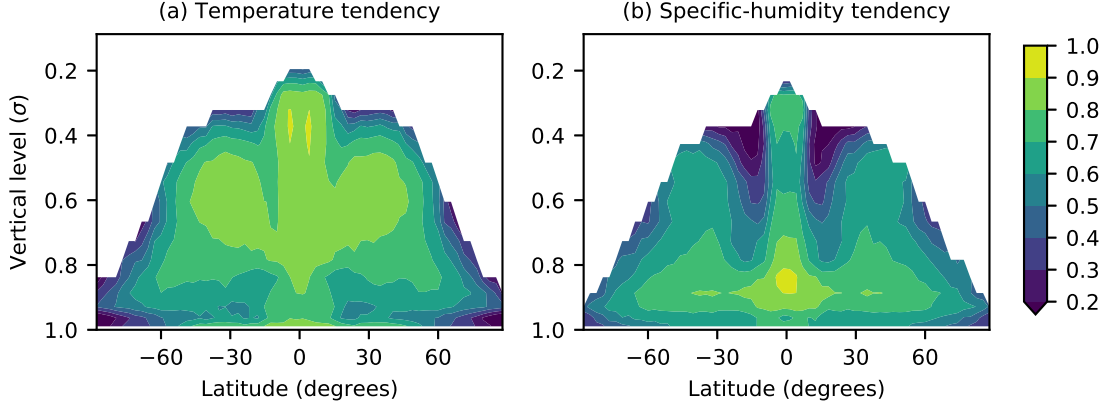
Figure 1. Coefficient of determination R^2 for the convective tendencies from the random forest (RF) trained on RAS convective tendencies in the control climate for (a) temperature and (b) specific humidity. Results are plotted versus latitude and vertical level (σ) since the underlying GCM is statistically zonally symmetric. R^2 is calculated based on the samples from the test dataset of the control climate (9900 samples for a given latitude and level), and it is only shown where the variance is at least 1% of the mean variance over all latitudes and levels.
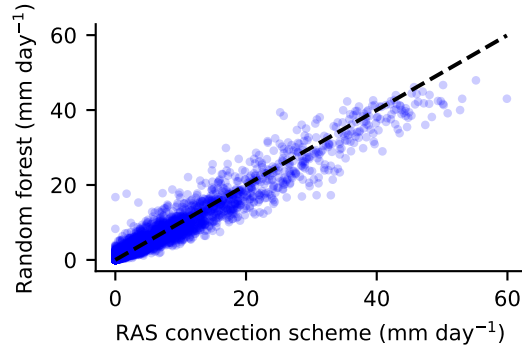

Figure 2. Scatterplot of instantaneous precipitation from the RAS parameterization versus the random forest (RF) trained on the control climate. Precipitation is the negative of the mass-weighted vertical integral of the specific humidity tendencies. The samples are from the test dataset for the control climate, and only a random subset of 10,000 samples are shown for clarity. The black dashed line is the one-to-one line. R^2 is 0.95 and the mean bias is negligible at 7×10^{-5} mm day^{-1}.

The nonlinear mapping that the RF learns may then be written as $\mathbf{y} = f(\mathbf{x})$, where the vector of features is $\mathbf{x} = (\mathbf{T}, \mathbf{q}, p_s)$ and the vector of scaled outputs is $\mathbf{y} = (c_p \partial \mathbf{T}/\partial t|_{\text{conv}}, L \partial \mathbf{q}/\partial t|_{\text{conv}})$. Here the vectors of temperature and specific humidity at different vertical levels are denoted $\mathbf{T}$ and $\mathbf{q}$, respectively, and p_s is the surface pressure. The time tendencies from convection are the output of the RAS convection scheme and are denoted $\partial \mathbf{T}/\partial t|_{\text{conv}}$ and $\partial \mathbf{q}/\partial t|_{\text{conv}}$ for temperature and specific humidity, respectively. Since convection is primarily active in the troposphere, we include the 21 σ-levels that satisfy $\sigma \geq 0.08$. Thus, there are 43 features and 42 outputs.

We choose to have only one RF that predicts the convective tendencies of both temperature and specific humidity at all the vertical levels considered, and thus there are 42 outputs

at each leaf of each tree. This column-based approach improves efficiency, and it ensures conservation of energy and non-negativity of precipitation as shown below. These two physical contraints would not hold if different RFs were used for predictions at each vertical level. Note also that we use the same RF for all latitudes (since RAS does not change depending on latitude) and that the RF is trained on data that includes both convecting and non-convecting gridpoints.

4.2 Training and test datasets

The temperature and specific humidity profiles and surface pressure were output and stored from the GCM once a day immediately prior to the point in the code at which RAS is called, and the convective tendencies of temperature and specific humidity calculated by RAS were also output and stored. We then randomly subsampled to 10 longitudes for a given time and latitude to make the samples effectively independent. Noting that the GCM is statistically zonally symmetric, time and longitude were combined into one sampling index, and the samples were then randomly shuffled in this index. The first 70% of the samples were stored for training while the remainder of the samples were stored as a test dataset for model assessment. Lastly, the training and test datasets were randomly subsampled so that the number of samples used at a given latitude is proportional to cosine of latitude to account for the greater surface area at lower latitudes. (Not including the cosine latitude factor in sampling does not strongly affect the quality of the fit.) The training samples were then aggregated across latitudes and reshuffled, such that the final training dataset depends only on sample index and level.

4.3 Fitting of Random Forest and choice of hyperparameters

To train the RF, we use the RandomForestRegressor class from the scikit-learn package version 0.18.1 [*Pedregosa et al.*, 2011]. An advantage of the RF approach is that there are only a few important hyper-parameters and they are relatively easy to tune. We analyzed the error of the RF using 10-fold cross-validation on the training dataset from the control climate. We varied the number of trees (*n_estimators*), the minimum number of samples required to be at each leaf node (*min_sample_leaf*), and the number of training samples used (*n_train*). Figures S1, S2, S3 in the Supporting Information show examples of the variations in error with these hyper-parameters. Over the ranges shown, the error decreases with increasing *n_estimators* but the decrease in error is not very great for values above ~ 5 (Fig. S1), the error decreases with increasing *n_train* but the decrease in error is not very great for values above ~ $500,000$ (Fig. S2), and the error is not very sensitive to *min_sample_leaf* (Fig. S3).

The final choice of hyperparameters involves a tradeoff between the desire to reduce error and the need for a fast parameterization that is not too large in memory when used in the GCM. In addition, we wanted to make sure that the size of the training dataset would be feasible for generation by a high-resolution convection-resolving or superparameterized model, with the caveat that training on the output of such models may differ from what is described here. Based on these considerations and the error analysis discussed above, we chose to use *n_estimators*=10, *min_sample_leaf*=10, and *n_train*=$700,000$. With the sampling approach described above, the training sample size is equivalent to just under 5 years of model output, but this could be reduced by sampling more often than once a day.

Using the above hyper-parameter choices, we fit RF models to the training samples from the control RAS simulation, the warm RAS simulation, and the combined training samples from the control and warm RAS simulations. In the combined case, we still used 700,000 samples, and these were chosen after random shuffling the combined dataset. The RF trained on the control simulation has an average number of nodes per tree of 62250, and it is 110Mb when stored as integers and single-precision floats in netcdf format for output to the GCM.

4.4 Validation on test dataset

The performance of the RF for the control climate as evaluated based on the test dataset is shown in Figs. 1 and 2. Note that the RF was not trained on any of the samples from the test dataset. We use the coefficient of determination R^2 which is defined as one minus the ratio of the mean squared error to the true variance. R^2 for the tendencies of temperature and specific humidity is above 0.8 in regions where the tendencies are large, such as the tropical mid-troposphere for temperature and the tropical lower troposphere for specific humidity, with generally higher R^2 for temperature as compared to specific humidity (Fig. 1). The overall R^2 for the RF is 0.82 as calculated over all test samples and levels, as compared to 0.86 for the training dataset. Note that the RF is specifically designed not to overfit the training data, in contrast to a single decision tree which could be trained to achieve perfect accuracy on a training dataset without achieving good performance on a test dataset.

The surface precipitation is also well captured by the RF (Fig. 2) with an R^2 of 0.95 and a negligible mean bias of 7×10^{-5} mm day^{-1}. The precipitation from RAS is the mass-weighted integral of the negative of the specific humidity tendency, and so precipitation does not require an additional prediction by the RF. Interestingly, the RF predictions of precipitation are reasonably accurate even at high values, and the ability of the RF to capture extremes of precipitation is discussed further in section 5.

The RF trained on the warm climate does similarly well in predicting the test dataset of the warm climate (Fig. S4) with R^2 of 0.77 for the tendencies and 0.93 for precipitation. Issues of generalization and application to climate change are discussed in section 6.

4.5 Conservation of energy and non-negative precipitation

As can be seen in Fig. 2, non-negativity of precipitation is ensured by the RF, and this holds because the predictions of the RF are means over select training samples that all have non-negative precipitation. Conservation of the column-integrated moist enthalpy, which is linear in temperature and specific humidity in the GCM, is also ensured for the same reason. The root-mean-squared error (RMSE) in conservation of column-integrated moist enthalpy in the control climate is very small at 0.2 W m^{-2} for both the training dataset and the RF predictions on the test dataset. This error in conservation with the RF is substantially smaller than errors of order 50-100 W m^{-2} that were reported recently for ANN parameterizations [*Brenowitz and Bretherton*, 2018; *Rasp et al.*, 2018], with the caveat that these reported conservation errors are not only due to errors in the ANNs and could be removed with a post-prediction adjustment.

5 Implementation in GCM and simulation of control climate

We discussed the performance of the RF in offline tests in the previous section. However, the most important test of a GCM parameterization is how it performs in simulations with the GCM. We consider the RF to be adequate as an emulator for climate studies if GCM simulations with the RF can reproduce the mean climate and higher-order statistics of simulations with the original parameterization. We also compare to simulations without any convective parameterization to give a benchmark for the magnitudes of any errors.

Routines to read in the RF (stored as a netcdf file as discussed above) and to use it to calculate convective tendencies were added to the GCM which is written in Fortran 90. These routines simply replace the RAS convection scheme where it is called in the GCM. Introducing the RF-based parameterization into the GCM did not create any problems with numerical instability in the GCM simulations. The RF is faster than RAS by a factor of three.

The performance of the GCM with the RF in simulating the control climate is shown in Fig. 3. Statistics are calculated using instantaneous four-times-daily output for temperature, winds and humidity. Daily accumulations are used for precipitation. The statistics shown are
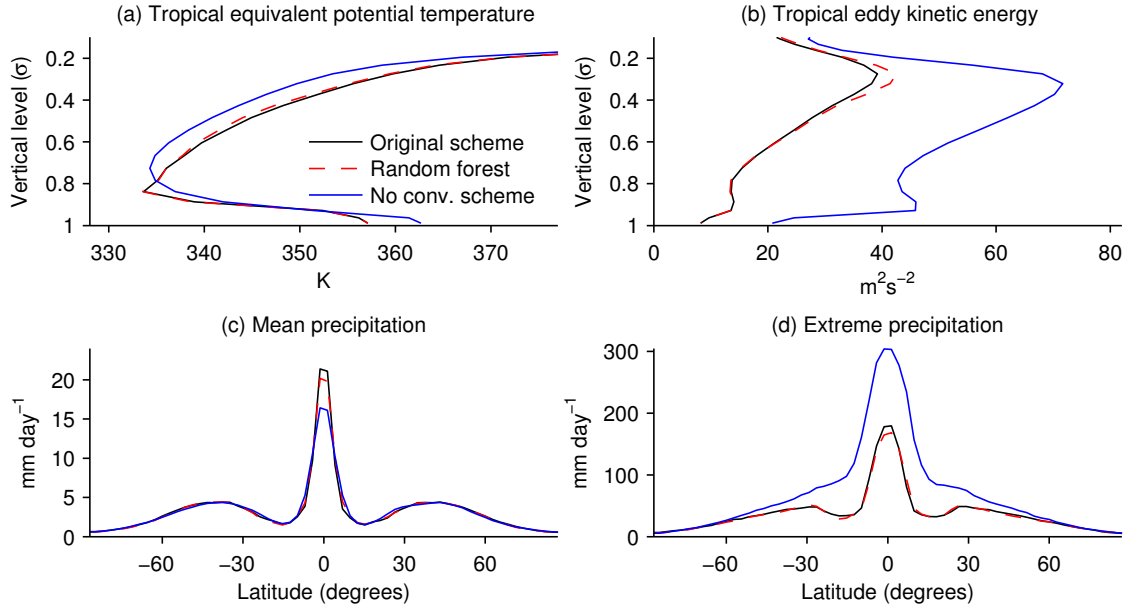
Figure 3.   Statistics from a GCM simulation of the control climate with the RAS parameterization (black) versus a simulation with the RF parameterization (red dashed) and a simulation without any convection scheme (blue). Shown are profiles of (a) tropical equivalent potential temperature versus vertical level (σ), (b) tropical eddy kinetic energy versus σ, (c) zonal- and time-mean precipitation versus latitude, and (d) the 99.9th percentile of daily precipitation versus latitude. Eddy kinetic energy is defined using eddy velocities with respect to the time and zonal mean. The tropical equivalent potential temperature and tropical eddy kinetic energy are based on zonal and time means that are then averaged (with area-weighting) over 20°S to 20°N.

the tropical-mean vertical profiles of equivalent potential temperature (θ_e) (Fig. 3a) and eddy activity as measured by the eddy kinetic energy (Fig. 3b), and the latitudinal distributions of mean precipitation (Fig. 3c) and extreme precipitation as measured by the 99.9th percentile of daily precipitation (Fig. 3d). In all cases, the GCM with the RF parameterization correctly captures the climate as compared to the GCM with the RAS parameterization (compare the black and dashed red lines in Fig. 3). This is particularly noteworthy for the tropical θ_e profile, tropical eddy kinetic energy, and extreme precipitation since these three statistics are sensitive to how convection is parameterized and behave quite differently in simulations in which the convection scheme is turned off and all convection must occur at the grid scale (compare the black and blue lines in Fig. 3a,b,d). Snapshots of daily precipitation in Fig. S5 illustrate that the RAS and RF parameterizations result in weaker precipitation extremes and more linear precipitation features in the intertropical convergence zone (ITCZ) as compared to the simulations without a convection scheme. Zonal and time-mean temperature is also well captured by the GCM with the RF parameterization with a RMSE of 0.3K over all latitudes and levels. The GCM with the RF parameterization generally does well for mean relative humidity, although the values are slightly too low in the tropical upper troposphere (Fig. S6).

Overall, these results suggest that the GCM with the RF parameterization can adequately simulate important climate statistics, including means, variances of winds (in terms of the eddy kinetic energy), and extremes. Climate statistics are the focus of this paper, but future work could evaluate the performance of the RF parameterization for other aspects such as wave propagation and initial value problems.

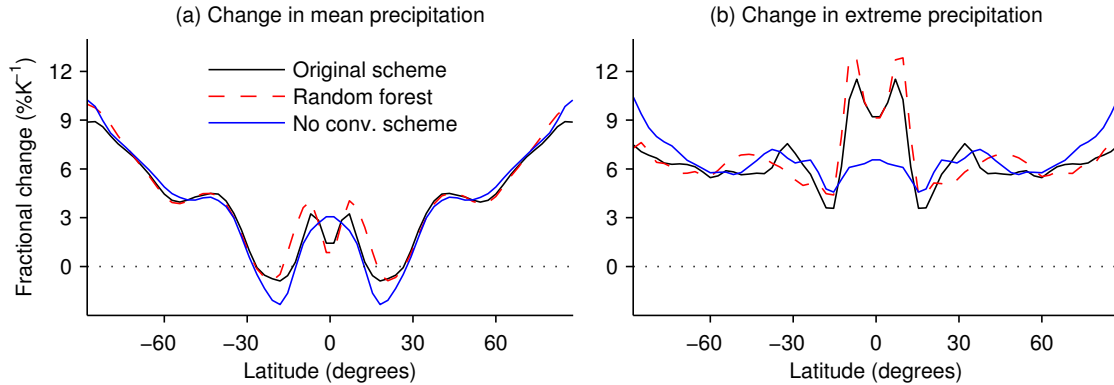## 6 Climate change and training in different climates

Figure 4. Changes in (a) zonal- and time-mean precipitation and (b) the 99.9th percentile of daily precipitation between the control climate and the warm climate for simulations with the RAS parameterization (black), with the RF parameterization (red dashed) and with no convection scheme (blue). Changes are expressed as the percentage change in precipitation normalized by the change in zonal- and time-mean surface-air temperature. The changes in this figure have been averaged between hemispheres, and a 1-2-1 filter has been applied to reduce noise.

We next assess the performance of the RF parameterization when applied to climate change. The RF introduces errors in simulating a given climate, and it is important to quantify the impact of these errors on the simulated response to a forcing. In addition, it is interesting to know whether an RF trained on a given climate can generalize to a different climate.

The most conservative approach is to train two RFs: one RF is trained on the control climate and used in a simulation of the control climate, and the other is trained on the warm climate and used in a simulation of the warm climate, and climate change is then calculated as the difference between the two climates. With this approach, the GCM with the RF parameterization accurately captures changes in climate, as shown for mean precipitation in Fig.4a and extreme precipitation in Fig. 4b. Note that RAS gives a strong increase in precipitation extremes in the tropics, albeit not as strong as when it was implemented in the GFDL coupled models CM2.0 and CM2.1 [*O'Gorman*, 2012]. The simulations in which the convection scheme is turned off have a more muted increase in extreme precipitation in the tropics. The GCM with the RF parameterization also faithfully captures the vertical and meridional structure of warming, with amplified warming in the tropical upper troposphere and polar amplification of warming in the lower troposphere (Fig. 5). The GCM with the RF parameterization is slightly less accurate for the changes in mean relative humidity (Fig.S7), but these are generally small except near the tropopause where the upward shift in the circulation and thermal structure combines with sharp vertical gradients in relative humidity to give large changes in relative humidity [cf. *Sherwood et al.*, 2010; *Singh and O'Gorman*, 2012].

Next we assess the performance of different RF training approaches for climate change as illustrated by the change in mean precipitation (Fig. 6). Results for the vertical profile of warming in the tropics are shown in Fig. S8 and lead to similar conclusions. When an RF is trained separately for each climate, the latitudinal profile of mean precipitation change is correctly captured (Fig. 6a, repeated from Fig. 4a). Training separately on different climates is not necessarily feasible for simulations of transient climate evolution. An alternative would be to train one RF using training data from a range of different climate states. We test this approach here by combining training data from the control and warm climates (but only us-
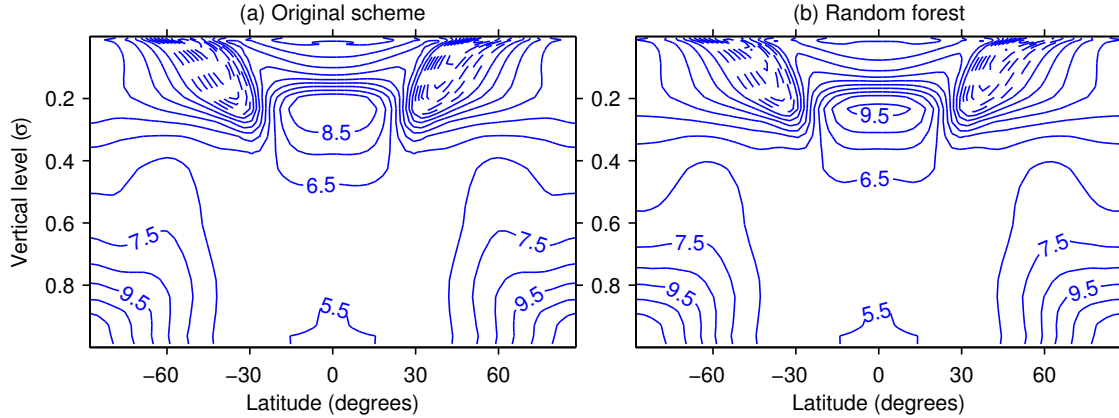
Figure 5. Change in zonal- and time-mean temperature (K) versus latitude and vertical level (σ) between the control climate and the warm climate for simulations with (a) the RAS parameterization and (b) the RF parameterization. The contour interval is 1K and negative contours are dashed. The temperature changes have been averaged between hemispheres. The difference between results shown in (a) and (b) over all latitudes and levels has a maximum absolute value of 1.1K and a root-mean-square value of 0.2K.

ing 700,000 training samples in total as before) and training one RF which is then used in GCM simulations of both climates. The GCM with the RF parameterization performs well in this case, as illustrated for the change in mean precipitation in Fig. 6b, and the control climate is also correctly simulated (not shown).

By contrast, training an RF on the control climate only and applying it in simulations of both the control climate and the warm climate leads to inaccurate climate-change results, with changes in precipitation in the tropics and subtropics that are incorrect and much too large (Fig. 6c). The RF fails to generalize because climate warming leads to higher temperatures and an upward shift of the circulation and thermal structure [*Singh and O'Gorman*, 2012] including the tropopause [*Vallis et al.*, 2015], but there are not examples in the training data from the control climate with such high temperatures or such a high tropopause as occur in the tropics of the warm climate. As a result, the vertical profile of tropical warming is severely distorted as shown in Fig. S8c. When the RF trained on the control climate is used to predict the convective temperature tendencies from the test dataset for the warm climate, it has no skill in the tropics equatorward of roughly 25° latitude (Fig. 7a). The cutoff latitude at which generalization fails may be estimated as the latitude at which the mean temperature in the warm climate is equal to the maximum mean temperature near the equator in the control climate. This estimate of the cutoff latitude is 19° for near-surface temperatures and 24° for temperatures at $\sigma = 0.5$, which is comparable to what would be inferred from Fig. 7a. Note however, that errors in the convective tendencies in the tropics are spread to other latitudes in the GCM simulations.

The climate-change considered here is large (increase in global-mean surface temperature of 6.5K) and generalization might be better for a smaller climate change. In addition, the control simulation does not have a seasonal cycle or ENSO-like variability, both of which might help by widening the range of training examples from the control climate. However, to the extent that an ML-based parameterization must extrapolate at least at some times when applied to a warmer climate (e.g., during warm ENSO events), we expect it will not perform well.

Interestingly, training the RF on the warm climate and then applying it in simulations of both the control and warm climates leads to good results for climate change (Fig. 6d). The
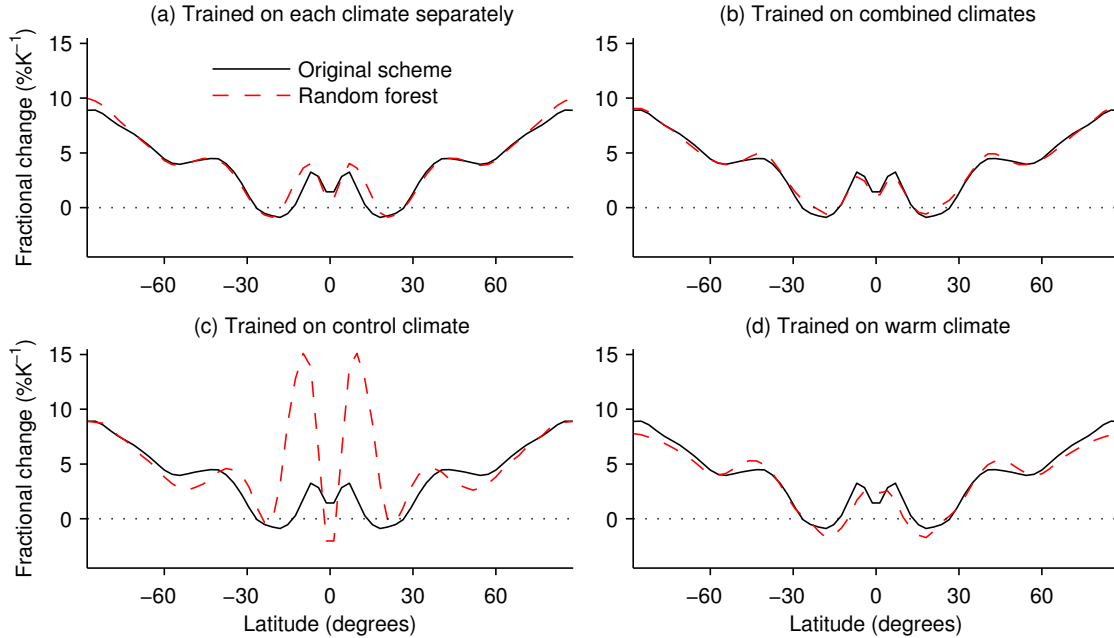
Figure 6. Impact of training on different climates for the response to climate change of zonal- and time-mean precipitation for the RAS parameterization (black) and the RF parameterization (dashed red): (a) a different RF is trained for each climate separately, (b) one RF is trained using combined training data from both climates, (c), one RF is trained using training data from the control climate only, and (d) one RF is trained using training data from the warm climate only. Changes are expressed as the percentage change in precipitation between the control and warm climate normalized by the change in zonal- and time-mean surface-air temperature. The changes in this figure have been averaged between hemispheres, and a 1-2-1 filter has been applied to reduce noise.

vertical profile of tropical warming is also well captured with a peak warming in the upper troposphere that is only slightly too strong (Fig. S8d). Convective tendencies from the test dataset of the control climate are well predicted by the RF trained on the warm climate except at polar latitudes where the tendencies are small in magnitude (Fig. 7b).

Why is climate change better simulated when training on the warm climate rather than the control climate? For a given latitude in the control climate with a certain surface temperature and tropopause height, it is possible to find training samples at higher latitudes in the warm climate with a similar tropopause height and surface temperature. Consistent with this argument, if training of the RF on the warm climate is limited to samples from the extratropics (latitudes poleward of 25° latitude in each hemisphere), it fails to predict the tropics of the warm climate as expected (Fig. 7c) but it still does a good job of predicting the tropics of the control climate (Fig. 7d). However, when training is based on the control climate, it is not possible to find training samples with a sufficiently high surface temperature and high tropopause that are needed for the tropics in the warm climate (Fig. 7a).

The asymmetry in the ability to generalize for climate cooling versus warming ultimately arises from differences between the tropics and extratropics. In the tropics, there is weak temperature variability and a warming climate quickly leads to problems for generalization. At high latitudes, moist convection is less important and there is more internal temperature variability which helps to broaden the range of training samples and makes it easier to generalize to a cooler climate. The meridional temperature gradient is also larger
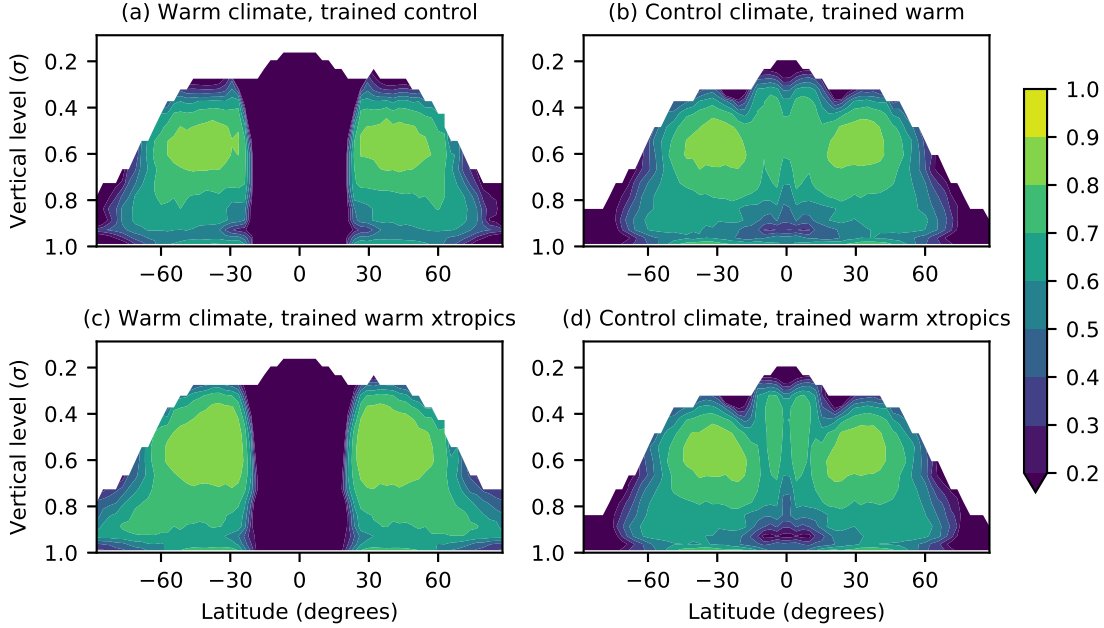
Figure 7. Generalization of the RF to different climates or latitude bands as measured by R^2 of the convective temperature tendencies: (a) test dataset from warm climate with RF trained on control climate, (b) test dataset from control climate with RF trained on warm climate, (c) test dataset from warm climate with RF trained on extratropics of warm climate, and (d) test dataset from control climate with RF trained on extratropics of warm climate. The extratropics is defined as latitudes poleward of 25° latitude in each hemisphere. R^2 is only shown where the variance is at least 1% of the mean variance over all latitudes and levels. The ability of the warm-climate RF to predict the tropics of the control climate as shown in (b) comes from the ability of extratropical samples in the warm climate to predict the tropics of the control climate as shown in (d).

outside the tropics which means that different surface temperatures can be reached by moving a smaller distance in latitude.

Overall, our results show that the RF parameterization performs well in simulations of climate change when the training data includes samples from both climates. An RF can be trained separately for each climate or the training data from both climates can be pooled to train one RF. Training on only the control climate gives poor results as might be expected. However, training on only the warm climate leads to remarkably good results for climate change, and this is because a given latitude in the control climate can be predicted by a higher latitude in the warm climate.

7 Feature importance of convection and sensitivity to perturbations

ML-based parameterizations could also be useful for building physical understanding about the interaction of convection with the large-scale temperature, humidity, and wind shear. Building an ML-based parameterization results in a nonlinear mapping that can be subsequently interrogated to learn about the underlying dynamics. We explore this possibility here in two different ways. First, we use the RF paramerization to generate a linear-response function for the response of convective precipitation to small perturbations in temperature, specific humidity and surface pressure. Second, we use the concept of "feature im-
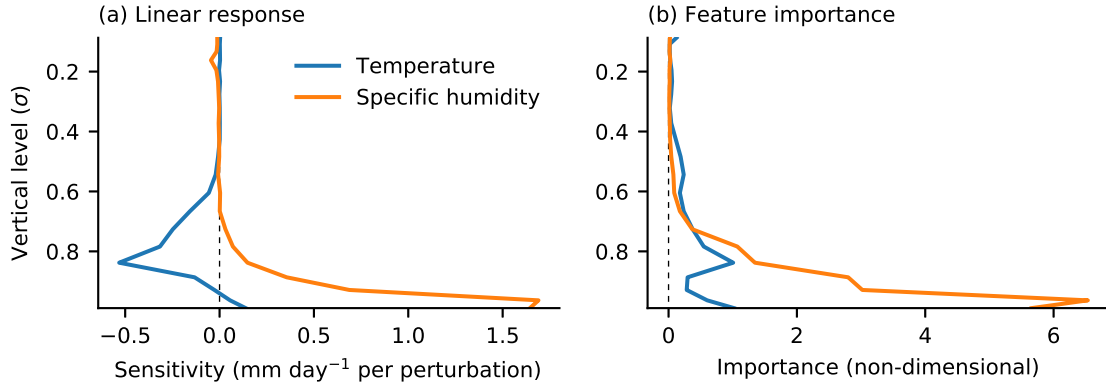
Figure 8. Diagnostics measuring the responsiveness of convective tendencies to input temperature (blue) and specific humidity (orange) at different vertical (σ) levels according to the RF parameterization trained on the control climate. (a) Sensitivity of surface precipitation in mm day^{-1} to perturbations in input temperature and specific humidity at different vertical levels (σ). The total perturbations are 1K for temperature and 1g kg^{-1} for specific humidity and these are applied to samples with non-zero precipitation from the test dataset. The sensitivities have been rescaled to approximately represent the response to a 50hPa-deep input perturbation centered at a given level. (b) Feature importance of input temperature and specific humidity at different σ levels for convection (including both occurrence and strength of convection). The importance values have been rescaled by $1/d\sigma$ to account for the uneven σ spacing. The vertically integrated importance is 0.24 for temperature and 0.75 for specific humidity (the importance of surface pressure is 0.01).

portance" which seeks to measure the importance of the different input features (here temperature and humidity at different levels and surface pressure) for the RF predictions [e.g., *Hastie et al.*, 2001]. The feature importance calculated here includes information on what features are important for both the occurrence and strength of convection, and it differs from the "importance profiles" discussed by *Mapes et al.* [2017] which we refer to here as linear response functions.

For both the linear response function and the feature importance, we present results for the RF trained on the control climate. These results are based on the RAS parameterization, and it would been possible to more directly calculate the linear response function of RAS without the intermediate step of the RF. However, if an RF is trained using high-resolution convection resolving simulations, the RF mapping could be directly interrogated without the need to run additional CRM simulations perturbed by forcings at different levels. And as we will show, the feature importance is a useful additional diagnostic for the interaction of convection with the large-scale environment.

7.1 Linear-response function

The linear-response function is similar to those that have previously constructed for moist convection based on CRM simulations or convective parameterizations [*Kuang*, 2010; *Herman and Kuang*, 2013; *Mapes et al.*, 2017]. The input temperature, specific humidity, and surface pressure of samples with non-zero precipitation from the test dataset of the control climate (including all latitudes) are systematically perturbed, and the RF is applied to the unperturbed and perturbed samples. For simplicity, the resulting changes in the predicted tendencies from the RF are measured by the perturbation in the predicted surface precipitation rate. The perturbations are added at each level and for each variable (temperature, humidity, or surface pressure) separately. The magnitude of the input perturbation is $dT = 0.5$K

for temperature, $dq = 0.5$g kg^{-1} for specific humidity, and $dp_s = 0.25$hPa for surface pressure. Both positive and negative perturbations are used, and the reported sensitivity is the precipitation for the positively perturbed input minus the precipitation for the negatively perturbed input (thus representing the response to total perturbations of 1K, 1g kg^{-1} and 0.5hPa) averaged across samples. The σ levels are unevenly spaced, and so the results for temperature and specific humidity at a given level are multiplied by $0.05/d\sigma$ to approximately represent the response to a 50hPa-deep input perturbation centered at that level. Note that the RF mapping is piecewise constant and not everywhere differentiable, but our perturbations are sufficiently large that this is not a problem for estimating the linear response function, and we have confirmed that the sensitivities are approximately doubled in size when the perturbations are doubled in size.

The linear response function is shown in Fig. 8a and is similar in some regards to what was found by *Mapes et al.* [2017] based on CRM simulations of unorganized convection in radiative-convective equilibrium at tropical temperatures. Note however that our results are for a convective parameterization in a full GCM simulation and including all latitudes; the maximum absolute values are greater and more similar to what is found by *Mapes et al.* [2017] if we only consider the equatorial region (not shown). Surface precipitation increases with moistening of the atmosphere, particularly at lower levels. This sensitivity is consistent with the positive effect of moisture on the buoyancy of a lifted parcel through both its initial moisture and the effect of entrainment of environmental air. However, the sensitivity to moistening is close to zero for levels above $\sigma = 0.7$, unlike what was found for CRM simulations by *Mapes et al.* [2017], and possibly indicative of a flaw that is common to convective parameterizations [*Derbyshire et al.*, 2004]. Surface precipitation increases for a near-surface warming, but decreases more strongly for a warming higher up, consistent with the effect of warming on the buoyancy of a parcel lifted from near the surface. For completeness, we note that the response to a surface pressure perturbation of 0.5hPa is 0.0015 mm day^{-1}.

7.2 Feature importance

Feature importance is shown in Fig. 8b based on the feature importance metric that is implemented in RandomForestRegressor class of scikit-learn (see *Hastie et al.* [2001] for a more general discussion). For a given feature, this metric measures the total decrease in mean-squared-error across nodes in a decision tree that split on that feature, weighting by the fraction of samples that reach a given node, and then averaged across trees in the ensemble. The resulting importance values are normalized to sum to one over all features. To account for the uneven spacing of the σ levels, we multiply the feature importance values for temperature and specific humidity by $1/d\sigma$. Similarly to the results from the linear response function, the results from the feature importance analysis imply that RAS precipitation is strongly sensitive to low-level moisture and to temperature near $\sigma = 0.8$. In addition, we find that moisture is generally more important than temperature, with the vertically integrated importance being 0.74 for specific humidity versus 0.24 for temperature (and surface pressure is not important at 0.01).

Advantages of feature importance compared to the linear response function include that it doesn't require an assumption of small perturbations and that it makes it easy to compare the importance of different variables (e.g., humidity versus temperature). Note that the linear response functions for temperature and specific humidity are not directly comparable because they assume a certain size of perturbation in each variable and they have different units. It would also be possible to calculate feature importances for a classifier trained on the occurrence of convection to determine which features are most important for the occurrence of convection separately from the strength of convection. On the other hand, the linear response function gives information on the sign of the response, and the magnitudes of the sensitivities are easier to interpret physically. Thus, both metrics are complementary and can be used together to gain insight from the ML parameterization into the interaction of convection with the environment.

8 Replacing both the large-scale condensation and convection schemes

So far we have chosen to replace the moist convection scheme with an ML algorithm and to continue using conventional parameterizations for the large-scale condensation, radiation, and boundary layer schemes. When training on the output of high-resolution models it would be possible to either allow the ML algorithm to represent all of these schemes in a GCM or to use it for only some of them. An advantage of replacing all of the schemes is that there can be significant compensation between tendencies from different schemes and there is not a clean physical separation of the different processes [e.g., *Arakawa*, 2004]. However, it could be argued that some of the processes are easier to represent accurately with a conventional parameterization.

To explore this issue, we also tried replacing the sum of tendencies from the moist convection scheme and the large-scale condensation scheme with an RF. Using the same approach to training the RF as described above was found to give poor results for relative humidity when the RF was implemented in the GCM (compare Fig. S6a and Fig. S9a), particularly in the extratropical upper troposphere where it can become negative since the GCM does not enforce positive humidity. We found through experimentation that the problem with the relative humidity was largely eliminated by adjusting the training approach to take into account the properties of the large-scale condensation scheme (Fig. S9b). We switched to relative humidity as the humidity input feature since large-scale condensation is sensitive to saturation, we switched the output scaling of the tendency of specific humidity to $L\sigma^{-3}$ instead of just L, to more strongly weight the upper troposphere where large-scale condensation is important for the relative humidity, and we removed the cosine latitude factor in the sampling used to generate training and test datasets since large-scale condensation is important at higher latitudes. All other aspects of the training and parameters of the RF remain the same.

The RF with this choice of sampling, features and output scaling correctly predicts the combined convective and large-scale condensation tendencies and surface precipitation when applied to the test dataset (Fig. S10 and S11), with an overall R^2 for the tendencies of 0.83 and for the precipitation of 0.93. When the RF is implemented in the GCM, replacing both the large-scale condensation and moist convection schemes, it leads to accurate simulations of the control climate (Fig. S12). However, the precipitation response to climate change is not accurate in the tropics (Fig. S13), possibly as a result of the need to simultaneously parameterize different processes at different vertical levels, but it would be worthwhile to further explore the best choices of features and output scalings for this case.

9 Conclusions

We have investigated how an RF-based parameterization of moist convection behaves when implemented in a GCM in an idealized setting. Encouragingly, the RF parameterization was found to lead to robust and accurate simulations of the control climate. The use of a decision-tree-based approach made it straightforward to ensure physical constraints such as energy conservation are preserved by the parameterization. Other approaches could be used to ensure physical constraints are obeyed (such as adding an adjustment to the predicted temperature tendencies to exactly conserve energy) but a decision tree approach is attractive in ensuring they are exactly satisfied to the extent that they hold in the training data. The RF parameterization was also found to perform well in the GCM in terms of simulation of extreme precipitation events, without the need for specialized training on those events.

Climate change was accurately simulated when training samples from both the control and warm climate were used, and combining the training samples from both climates to train one RF was adequate. However, the RF trained in the control climate did not generalize to the warm climate, and the cutoff latitude at which it failed to generalize is approximately equal to the latitude at which the mean temperature in the warm climate is equal to the max-

imum mean temperature near the equator in the control climate. Remarkably, training on just the warm climate gave good results for climate change. In effect, a given latitude in the control climate is predicted by samples from higher latitudes in the warm climate. The asymmetry between generalization for a warming versus a cooling climate relates to the weaker internal temperature variability, weaker meridional temperature gradients, and greater importance of moist convection in the tropics versus higher latitudes.

We have also illustrated how an ML parameterization can be interrogated to learn about underlying physical processes. First, the RF parameterization is useful as a means to efficiently generate linear response functions for small perturbations. Second, the RF parameterization can be use to measure the importance of different environmental variables such as temperature and humidity at different levels for convection, without the need to assume small perturbations. Feature importance could be further investigated separately for the occurrence of convection and the intensity of convection when it is occurring.

The setting we have used is idealized both in terms of using an aquaplanet GCM and in terms of learning from a conventional parameterization rather than from high-resolution simulations. Other studies have demonstrated that learning from CRM simulations or superparameterized models is feasible [*Krasnopolsky et al.*, 2013; *Brenowitz and Bretherton*, 2018; *Gentine et al.*, 2018; *Rasp et al.*, 2018]. When training on resolved convection rather than a conventional parameterization, processing is needed to calculate the appropriate convective tendencies to train on (e.g., through coarse-graining approaches) and the interpretation of feature importance and linear response functions are complicated by the presence of other dynamical processes in addition to moist convection. Some of the interesting issues that remain to be explored include whether an ML parameterization should be non-local in space and time, whether it should be applied in addition to boundary-layer, radiation and large-scale cloud schemes or replace all of these, and the extent to which convective-momentum tendencies can be predicted. Feature engineering, akin to our use of relative humidity and a vertical weighting function in section 8, is likely to be useful in achieving good performance. Extending to a more realistic GCM with land brings up additional technical problems such as the strong diurnal cycle over land and the need to predict convection at different elevations in the presence of topography. These are non-trivial challenges, but our results suggest that the use of ML is promising both for development of new parameterizations and for new diagnostics of the interaction of subgrid processes with the large-scale.

References

Anderson, J. L., et al. (2004), The new GFDL global atmosphere and land model AM2–LM2: Evaluation with prescribed SST simulations, *J. Climate*, *17*, 4641–4673.

Arakawa, A. (2004), The cumulus parameterization problem: Past, present, and future, *J. Climate*, *17*, 2493–2525.

Arakawa, A., and W. H. Schubert (1974), Interaction of a cumulus cloud ensemble with the large-scale environment, Part I, *J. Atmos. Sci.*, *31*, 674–701.

Bechtold, P., M. Köhler, T. Jung, F. Doblas-Reyes, M. Leutbecher, M. J. Rodwell, F. Vitart, and G. Balsamo (2008), Advances in simulating atmospheric variability with the ECMWF model: From synoptic to decadal time-scales, *Quart. J. Roy. Meteorol. Soc.*, *134*, 1337–1351.

Belochitski, A., P. Binev, R. DeVore, M. Fox-Rabinovitz, V. Krasnopolsky, and P. Lamby (2011), Tree approximation of the long wave radiation parameterization in the NCAR CAM global climate model, *J. Comput. Appl. Math.*, *236*, 447–460.

Benedict, J. J., E. D. Maloney, A. H. Sobel, D. M. Frierson, and L. J. Donner (2013), Tropical intraseasonal variability in version 3 of the GFDL atmosphere model, *J. Climate*, *26*, 426–449.

Breiman, L. (2001), Random forests, *Machine learning*, *45*, 5–32.

Brenowitz, N. D., and C. S. Bretherton (2018), Prognostic validation of a neural network unified physics parameterization, *Geophys. Res. Lett.*, *45*, 6289–6298.

Chevallier, F., F. Chéruy, N. A. Scott, and A. Chédin (1998), A neural network approach for a fast and accurate computation of a longwave radiative budget, *J. App. Meteorol.*, *37*, 1385–1397.

Derbyshire, S. H., I. Beau, P. Bechtold, J. Y. Grandpeix, J. M. Piriou, J. L. Redelsperger, and P. M. M. Soares (2004), Sensitivity of moist convection to environmental humidity, *Quart. J. Roy. Meteorol. Soc.*, *130*, 3055–3079.

Dwyer, J. G., and P. A. O'Gorman (2017), Moist formulations of the Eliassen–Palm flux and their connection to the surface westerlies, *J. Atmos. Sci.*, *74*, 513–530.

Emanuel, K. A., and M. Živković-Rothman (1999), Development and evaluation of a convection scheme for use in climate models, *J. Atmos. Sci.*, *56*, 1766–1782.

Farneti, R., and P. R. Gent (2011), The effects of the eddy-induced advection coefficient in a coarse-resolution coupled climate model, *Ocean Model.*, *39*, 135–145.

Frierson, D. M. W., I. M. Held, and P. Zurita-Gotor (2006), A gray-radiation aquaplanet moist GCM. Part I: Static stability and eddy scale, *J. Atmos. Sci.*, *63*, 2548–2566.

Gentine, P., M. Pritchard, S. Rasp, G. Reinaudi, and G. Yacalis (2018), Could machine learning break the convection parameterization deadlock?, *Geophys. Res. Lett.*, *45*, 5742–5751.

Hastie, T., R. Tibshirani, and J. Friedman (2001), *The elements of statistical learning*, 2nd ed., 745 pp., Springer.

Held, I. M., M. Zhao, and B. Wyman (2007), Dynamic radiative–convective equilibria using GCM column physics, *J. Atmos. Sci.*, *64*, 228–238.

Herman, M. J., and Z. Kuang (2013), Linear response functions of two convective parameterization schemes, *J. Adv. Model Earth. Syst.*, *5*, 510–541.

Khairoutdinov, M. F., and D. A. Randall (2001), A cloud resolving model as a cloud parameterization in the NCAR Community Climate System Model: Preliminary results, *Geophys. Res. Lett.*, *28*, 3617–3620.

Kim, D., A. H. Sobel, A. D. Del Genio, Y. Chen, S. J. Camargo, M.-S. Yao, M. Kelley, and L. Nazarenko (2012), The tropical subseasonal variability simulated in the NASA GISS general circulation model, *J. Climate*, *25*, 4641–4659.

Kooperman, G. J., M. S. Pritchard, M. A. Burt, M. D. Branson, and D. A. Randall (2016), Robust effects of cloud superparameterization on simulated daily rainfall intensity statistics across multiple versions of the Community Earth System Model, *J. Adv. Model. Earth. Sy.*, *8*, 140–165.

Krasnopolsky, V. M. (2013), *The application of neural networks in the earth system sciences*, 189 pp., Springer.

Krasnopolsky, V. M., M. S. Fox-Rabinovitz, H. L. Tolman, and A. A. Belochitski (2008), Neural network approach for robust and fast calculation of physical processes in numerical environmental models: Compound parameterization with a quality control of larger errors, *Neural Netw.*, *21*, 535–543.

Krasnopolsky, V. M., M. S. Fox-Rabinovitz, and A. A. Belochitski (2010), Development of neural network convection parameterizations for numerical climate and weather prediction models using cloud resolving model simulations, in *The 2010 International Joint Conference on Neural Networks (IJCNN)*, pp. 1–8, IEEE.

Krasnopolsky, V. M., M. S. Fox-Rabinovitz, and A. A. Belochitski (2013), Using ensemble of neural networks to learn stochastic convection parameterizations for climate and numerical weather prediction models from data simulated by a cloud resolving model, *Adv. Artif.*

Neural Syst., *2013*, Article ID 485913.

Kuang, Z. (2010), Linear response functions of a cumulus ensemble to temperature and moisture perturbations and implications for the dynamics of convectively coupled waves, *J. Atmos. Sci.*, *67*, 941–962.

Ling, J., A. Kurzawski, and J. Templeton (2016), Reynolds averaged turbulence modelling using deep neural networks with embedded invariance, *J. Fluid Mech.*, *807*, 155–166.

Mapes, B., and R. Neale (2011), Parameterizing convective organization to escape the entrainment dilemma, *J. Adv. Model Earth. Syst.*, *3*(M06004).

Mapes, B., A. S. Chandra, Z. Kuang, and P. Zuidema (2017), Importance profiles for water vapor, *Surv. Geophys.*, *38*, 1355–1369.

Monteleoni, C., G. A. Schmidt, F. Alexander, A. Niculescu-Mizil, K. Steinhaeuser, M. Tippett, A. Banerjee, M. B. Blumenthal, A. R. Ganguly, J. E. Smerdon, and M. Tedesco (2013), Climate informatics, in *Computational Intelligent Data Analysis for Sustainable Development*, edited by T. Yu, N. Chawla, and S. Simoff, chap. 4, pp. 81–126, CRC Press.

Moorthi, S., and M. J. Suarez (1992), Relaxed Arakawa-Schubert: A parameterization of moist convection for general circulation models, *Mon. Weather Rev.*, *120*, 978–1002.

O'Gorman, P. A. (2011), The effective static stability experienced by eddies in a moist atmosphere, *J. Atmos. Sci.*, *68*, 75–90.

O'Gorman, P. A. (2012), Sensitivity of tropical precipitation extremes to climate change, *Nature Geo.*, *5*, 697–700.

O'Gorman, P. A., and J. G. Dwyer (2018), Training and testing data, associated code, and estimators for emulating a convection scheme, doi:10.5281/zenodo.1434401, https://doi.org/10.5281/zenodo.1434401.

O'Gorman, P. A., and T. Schneider (2008), The hydrological cycle over a wide range of climates simulated with an idealized GCM, *J. Climate*, *21*, 3815–3832.

O'Gorman, P. A., and T. Schneider (2009), Scaling of precipitation extremes over a wide range of climates simulated with an idealized GCM, *J. Climate.*, *22*, 5676–5685.

Pedregosa, F., G. Varoquaux, A. Gramfort, V. Michel, B. Thirion, O. Grisel, M. Blondel, P. Prettenhofer, R. Weiss, V. Dubourg, J. Vanderplas, A. Passos, D. Cournapeau, M. Brucher, M. Perrot, and É. Duchesnay (2011), Scikit-learn: Machine learning in Python, *J. Mach. Learn. Res.*, *12*, 2825–2830.

Randall, D., M. Khairoutdinov, A. Arakawa, and W. Grabowski (2003), Breaking the cloud parameterization deadlock, *Bull. Amer. Meteor. Soc.*, *84*, 1547–1564.

Rasp, S., M. S. Pritchard, and P. Gentine (2018), Deep learning to represent sub-grid processes in climate models, *Proc. Natl. Acad. Sci.*, doi:10.1073/pnas.1810286115.

Schneider, T., S. Lan, A. Stuart, and J. Teixeira (2017), Earth System Modeling 2.0: A blueprint for models that learn from observations and targeted high-resolution simulations, *Geophys. Res. Lett.*, *44*, 12,396–12,417.

Sherwood, S. C., W. Ingram, Y. Tsushima, M. Satoh, M. Roberts, P. L. Vidale, and P. A. O'Gorman (2010), Relative humidity changes in a warmer climate, *J. Geophys. Res.*, *115*, D09,104.

Singh, M. S., and P. A. O'Gorman (2012), Upward shift of the atmospheric general circulation under global warming: Theory and simulations, *J. Climate*, *25*, 8259–8276.

Stevens, B., and S. Bony (2013), What are climate models missing?, *Science*, *340*, 1053–1054.

Vallis, G. K., P. Zurita-Gotor, C. Cairns, and J. Kidston (2015), Response of the large-scale structure of the atmosphere to global warming, *Quart. J. Roy. Meteorol. Soc.*, *141*, 1479–1501.

Wang, J.-X., J.-L. Wu, and H. Xiao (2017), Physics-informed machine learning approach for reconstructing Reynolds stress modeling discrepancies based on DNS data, *Phys. Rev. Fluids*, *2*, 034603.

Wilcox, E. M., and L. J. Donner (2007), The frequency of extreme rain events in satellite rain-rate estimates and an atmospheric general circulation model, *J. Climate*, *20*, 53–69.